A MODEL FOR RESIDUAL STRESS AND PART WARPAGE PREDICTION IN MATERIAL EXTRUSION WITH APPLICATION TO POLYPROPYLENE

N. Watanabe[1], M. L. Shofner[2], N. Treat[3], and D. W. Rosen[1]*

[1]George W. Woodruff School of Mechanical Engineering, Georgia Institute of Technology, Atlanta, GA 30332
[2]School of Materials Science and Engineering, Georgia Institute of Technology, Atlanta, GA 30332
[3]IMERYS Filtration & Performance Additives, San Jose, CA 95134

*Corresponding author. Email: david.rosen@me.gatech.edu

Abstract

The layer-by-layer fabrication procedure causes residual stresses to accumulate due to the repetition of heating and cooling during the material extrusion process. In this study, residual stress and part warpage of a polypropylene copolymer are investigated. The effects of adjusting process variable settings, such as deposition temperature, deposition speed, and layer height, on part warpage are analyzed computationally and experimentally. Material extrusion process simulation models that are capable of predicting the temperature distributions, deposited filament shapes, and residual stresses of fabricated parts have been developed. These models are used to predict the warpages and deformations of the fabricated parts; these predictions are compared with experimental results to evaluate the models' efficacy. Insights are gained on the effects of particulate inclusions on the residual stress and warpage behaviors of polypropylene copolymer.

Introduction

During the material extrusion process, the part goes through a repetition of heating and cooling as the filament is liquefied in the liquefier chamber and is deposited onto a build platform to fabricate a three-dimensional part. This layer-by-layer fabrication procedure causes residual stresses to accumulate in the part. This study focuses on thermally-induced residual stress caused by the crystallization of the material during the cooling process, which leads to part warpage.

One of the challenges in material extrusion additive manufacturing is the limited availability of materials. With additive manufacturing processes, many of the part geometries that are unachievable using conventional manufacturing processes can be realized. As different material compositions are investigated, additive manufacturing technology will be improved even further by expanding the portfolio of available materials. Polypropylene, a widely used thermoplastic that is inexpensive and flexible compared to acrylonitrile-*co*-butadiene-*co*-styrene (ABS), is the material of interest of this study. However, polypropylene is a semi-crystalline thermoplastic unlike ABS, which is an amorphous thermoplastic, and there are processing issues associated with material extrusion of polypropylene. As shown in Figure 1, the molecules in semi-crystalline thermoplastics are drawn together and ordered during the

crystallization process, so they shrink more compared to amorphous thermoplastics. This causes parts that are fabricated with polypropylene to warp more and detach from the build platform, compared to those with ABS.
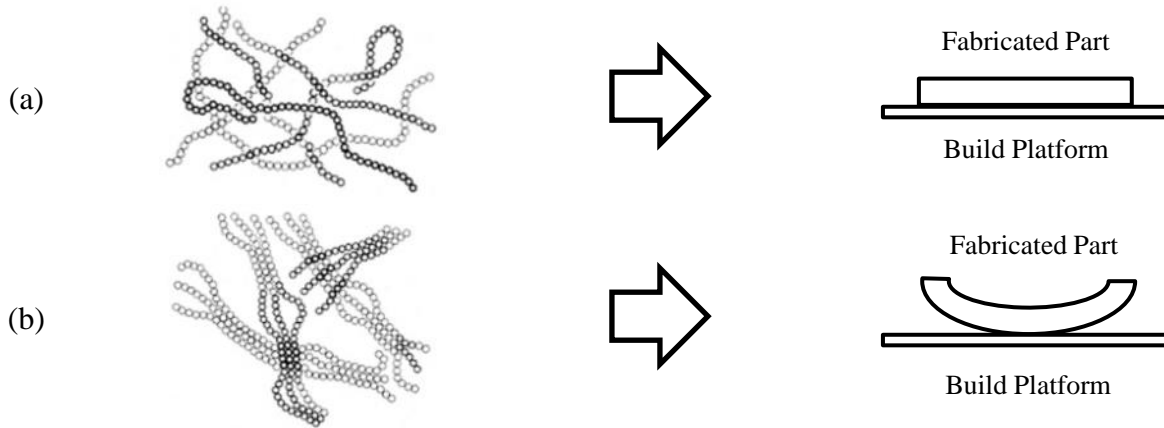
Fig. 1 Schematic representation of molecules and fabricated parts of (a) amorphous thermoplastics and (b) semi-crystalline thermoplastics [1]

      Alternatives to reduce warpage are to create polypropylene-based composite materials by combining polypropylene with additives and/or investigate polypropylene copolymers with reduced crystallinity. Several types of additives exist, such as particles, fibers, and agents that affect viscosity and thermal conductivity. Although this allows for a large variety of possible composite materials, trying to create new materials requires a vast amount of effort and time and can be expensive. In order to make this process quicker and more cost effective, computational methods are required instead of solely relying on iterative experiments. Therefore, the objective of this research is to develop material extrusion process simulation models that are capable of predicting the temperature distributions, deposited filament shapes, residual stresses, and warpages/deformations of fabricated parts, where the inputs are material properties, process variable settings, and process conditions. A commercially available polypropylene copolymer was used here as a model system for study. The simulation model overview is presented in Figure 2.
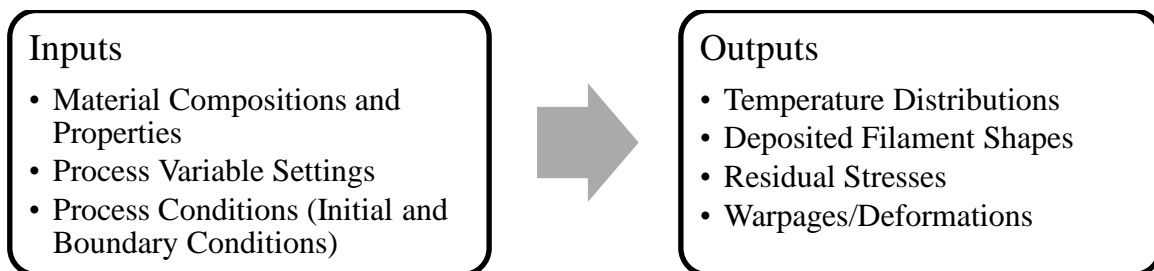
Fig. 2 Overview of material extrusion process simulation models

Material Properties

Although it is convenient to consider the liquification and extrusion process to be isothermal, temperature variations can and do occur throughout the process. Material properties need to be considered as a function of temperature in this case [2]. In this research, a combined theoretical and experimental approach was taken to characterize the flow characteristics of the materials, where a known model for the viscosity was compared to experimental viscosity data obtained from a capillary rheometer.

Viscosity controls much of the material's behavior through the liquefier. The approach used here begins with the assumption that material extrusion materials are shear-thinning and follow a power-law viscosity model as shown in Equation 1:

$$\eta = K(\dot{\gamma})^{n-1} \tag{1}$$

where η is viscosity, $\dot{\gamma}$ is shear rate, and K and n are power-law fit parameters. In order to account for the temperature dependence of viscosity, Bellini et al. [3] suggested separating the viscosity expression into temperature and shear-rate dependent terms as follows in Equation 2:

$$\eta = H(T)\eta_{T_o}(\dot{\gamma}) \tag{2}$$

The latter shear-rate dependent term is typically taken as the power-law expression evaluated at a reference temperature, T_α. The temperature dependent term is typically assumed to be described by an Arrhenius model as shown in Equation 3:

$$H(T) = e^{\left[\alpha\left(\frac{1}{T}-\frac{1}{T_\alpha}\right)\right]} \tag{3}$$

where α is the activation energy.

Experiments were conducted on a capillary rheometer to obtain viscosity data at various shear rates and temperatures. Using the standard models described above, a viscosity expression that depended on shear rate and temperature was determined for the polypropylene copolymer. The resultant viscosity surface plot was created at shear rates representative of the material extrusion process (100 to 10,000 s^{-1}) and temperatures from 200 °C to 260 °C and is presented in Figure 3. This shows that viscosity decreased as temperature and shear rate increased.
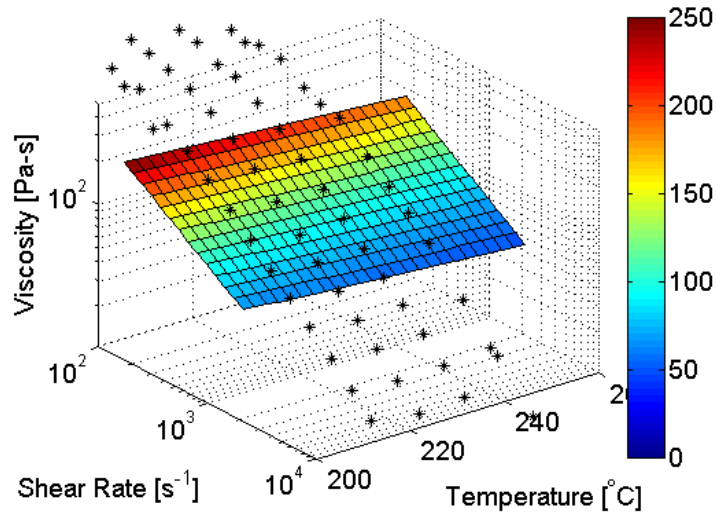
Fig. 3 Viscosity surface plot of polypropylene copolymer

There were several other critical material properties that were used as inputs to the simulation models, and those for the polypropylene copolymer are summarized and presented in Table 1.

Table 1 Material properties of polypropylene copolymer

Viscosity Expression	$\eta = e^{\left[1318.9\left(\frac{1}{T}-\frac{1}{503.15}\right)\right]}3346.4(\dot{\gamma})^{-0.54}$
Coefficient of Thermal Expression	1.50×10^{-4} m/(m-°C)
Thermal Conductivity	0.2 W/(m-°C)
Specific Heat	1920 J/(kg-°C)
Density	900 kg/m^3
Melting Temperature (T_m)	151.0 °C
Crystallization Temperature (T_c)	104.0 °C

Material Extrusion Additive Manufacturing Machine

The material extrusion additive manufacturing machine that was used in this research is called HYREL System 30 from HYREL 3D [4]. This is a versatile material extrusion machine, which is capable of fabricating high quality parts and supporting research and development of extrusion materials and technologies. The hardware and software are meant to be open, enabling users to have complete control over the extrusion process. The HYREL machine consists of over twenty adjustable settings, which can be fine-tuned to facilitate deposition of a wide range of materials. For example, one of the drive rollers in the printhead is spring-mounted, which enables a constant normal force to be exerted on the filament even if the filament diameter varies. This facilitates material development research, since the requirements on making uniform filaments are not as stringent as for filament production.

In this research, the effects of adjusting process variable settings, such as deposition temperature, deposition speed, and layer height, on part warpage were analyzed computationally

and validated experimentally. The process variable settings that are representative of the material extrusion process were selected and used as inputs to the simulation models. These values are presented in Table 2.

Table 2 Process variable settings for process simulation models

| Process Variable Settings	Simulation Model Input Values		
Deposition Temperature	200 °C	220 °C	240 °C
Deposition Speed	10 mm/s	20 mm/s	30 mm/s
Layer Height	0.1 mm	0.2 mm	0.3 mm

Material Extrusion Process Simulation Models

The development of two-dimensional material extrusion process simulation models using ANSYS® Polyflow and Mechanical is described in this section. To capture the thermal processes experienced during material deposition, several simulations were developed, and these sequential simulations were linked to one another through the temperature profiles developed in previous steps.

The first simulation model was the deposition and cooling of the first layer of filament. The first layer was deposited onto a build platform, which was assumed to be at a constant temperature of 80 °C. The geometry and mesh before the deposition is shown in Figure 4. The volumetric flow rate at the nozzle, Q, is calculated using Equation 4:

$$Q = v_r W H \tag{4}$$

where v_r is the deposition velocity, W is the width of the deposited road, and H is its height, assuming that the deposited filament had more of a rectangular shape than circular [5]. By applying the calculated volumetric flow rate at the nozzle entrance and gravitational force, and using the remeshing technique in ANSYS® Polyflow, the deposition of the first layer was performed. In this simulation model, the filament was extruded through the nozzle in the vertical direction, while the deposition velocity was applied in the horizontal direction. In order to simulate the relative motion between the nozzle and the build platform, the nozzle was maintained in a fixed position, while the build platform translated in the horizontal direction with a deposition velocity.
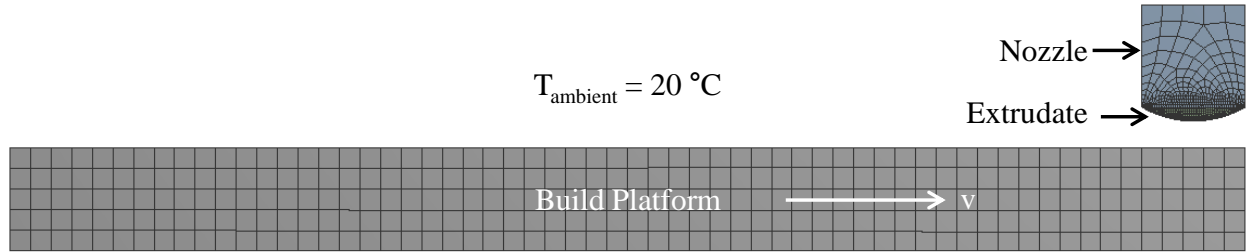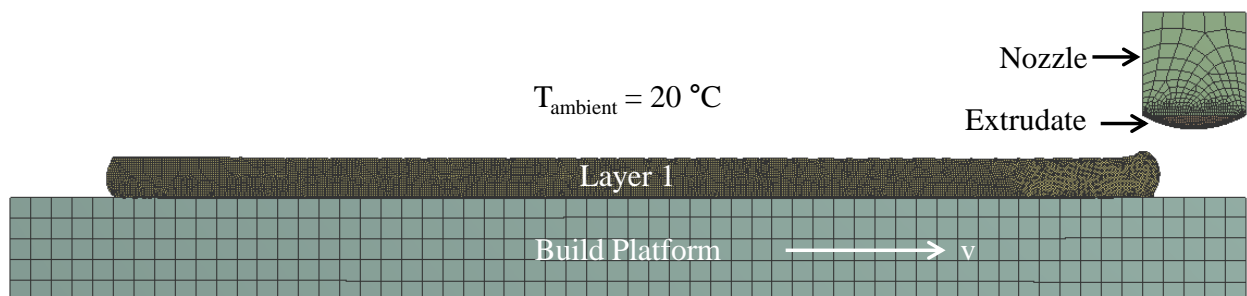
Fig. 4 Geometry and mesh before the first layer deposition

The geometry and mesh before the cooling of the first layer of filament is presented in Figure 5. The temperature distribution and deposited filament shape after the first layer deposition were exported from the previous stage of the simulation model. The build platform temperature was applied to the bottom surface of the first layer, and the other surfaces were subjected to cooling due to convection with air.
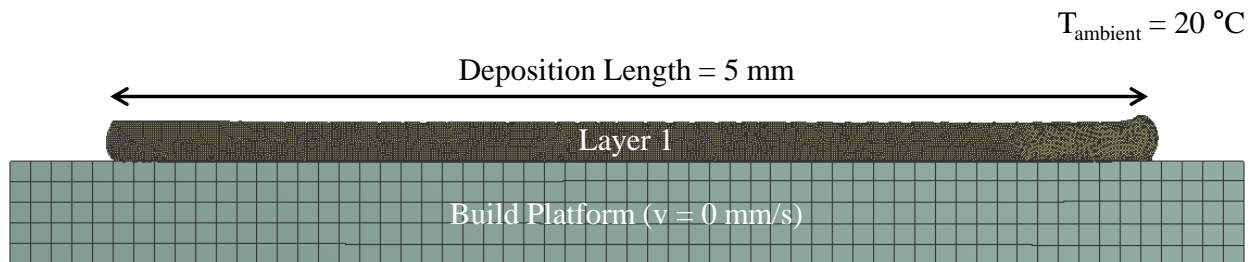

Fig. 5 Geometry and mesh before the first layer cooling

The second simulation model was the deposition of the second layer of filament on top of the first layer and the cooling of both layers. Once again, the temperature distribution after the first layer cooling was exported from the previous simulation, and the geometry and mesh before the second layer deposition is shown in Figure 6. The procedure for this simulation model was similar to that for the first layer deposition and cooling. However, it was crucial to simulate the conduction heat transfer between the two layers in this stage. This was accomplished using the fluid-to-fluid contact capability in ANSYS® Polyflow.

Fig. 6 Geometry and mesh before the second layer deposition

The last simulation model determined the residual stress and warpage/deformation of the deposited two layers of filaments. The exported temperature distributions and deposited filament shapes were imported into ANSYS® Mechanical to conduct structural analyses. By fixing the mid-point on the bottom surface of the first layer to the build platform, and applying zero force everywhere else, the residual stress and warpage during the cooling process were computed.

$T_{ambient} = 20\ °C$

Force = 0
Everywhere else

Layer 2
Layer 1
Fixed at this point
Build Platform
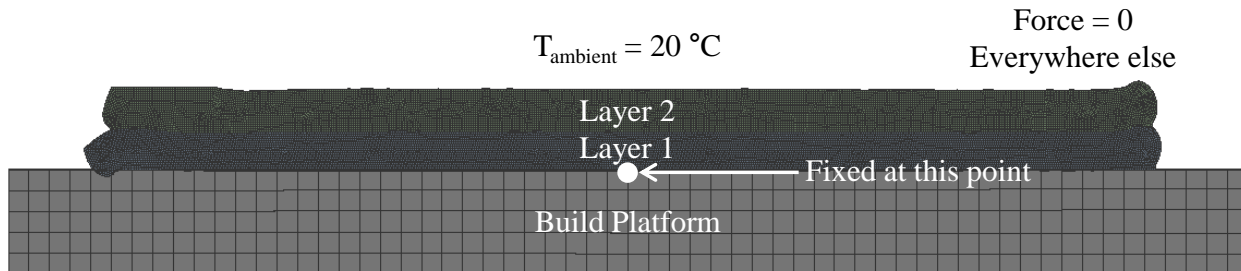
Fig. 7 Geometry and mesh before the residual stress/warpage simulation

Results

The results from each material extrusion process simulation model with one set of process variable settings are presented in this section. The selected values for deposition temperature, deposition speed and layer height were 220 °C, 20 mm/s and 0.2 mm, respectively. These represent average values of process variable settings that are representative of the material extrusion process as shown in Table 2.

The evolution of temperature distribution and deposited filament shape during the first layer deposition is shown in Figure 8. The results are compared to material extrusion of ceramics conducted by Bellini as shown in Figure 9 [6]. There were several differences between the two simulation models, and they are also summarized in Table 3. The critical differences that had impacts on the temperature distribution results were the heat transfer coefficient of the build platform and the deposition speed. A lower heat transfer coefficient was used in Bellini's model due to the differences in the build platform material between the two models. The build platform was assumed to be made of insulated foam in Bellini's model, whereas a glass build platform was used in this study. A lower value caused slower cooling at the bottom surface of the first layer, which resulted in a smaller temperature difference between the top and bottom surfaces. In addition, a lower deposition speed was used in Bellini's model, which resulted in a smaller temperature difference in the deposition direction. These differences impacted the temperature profile in the extruded filament, as shown in Figures 8 and 9.
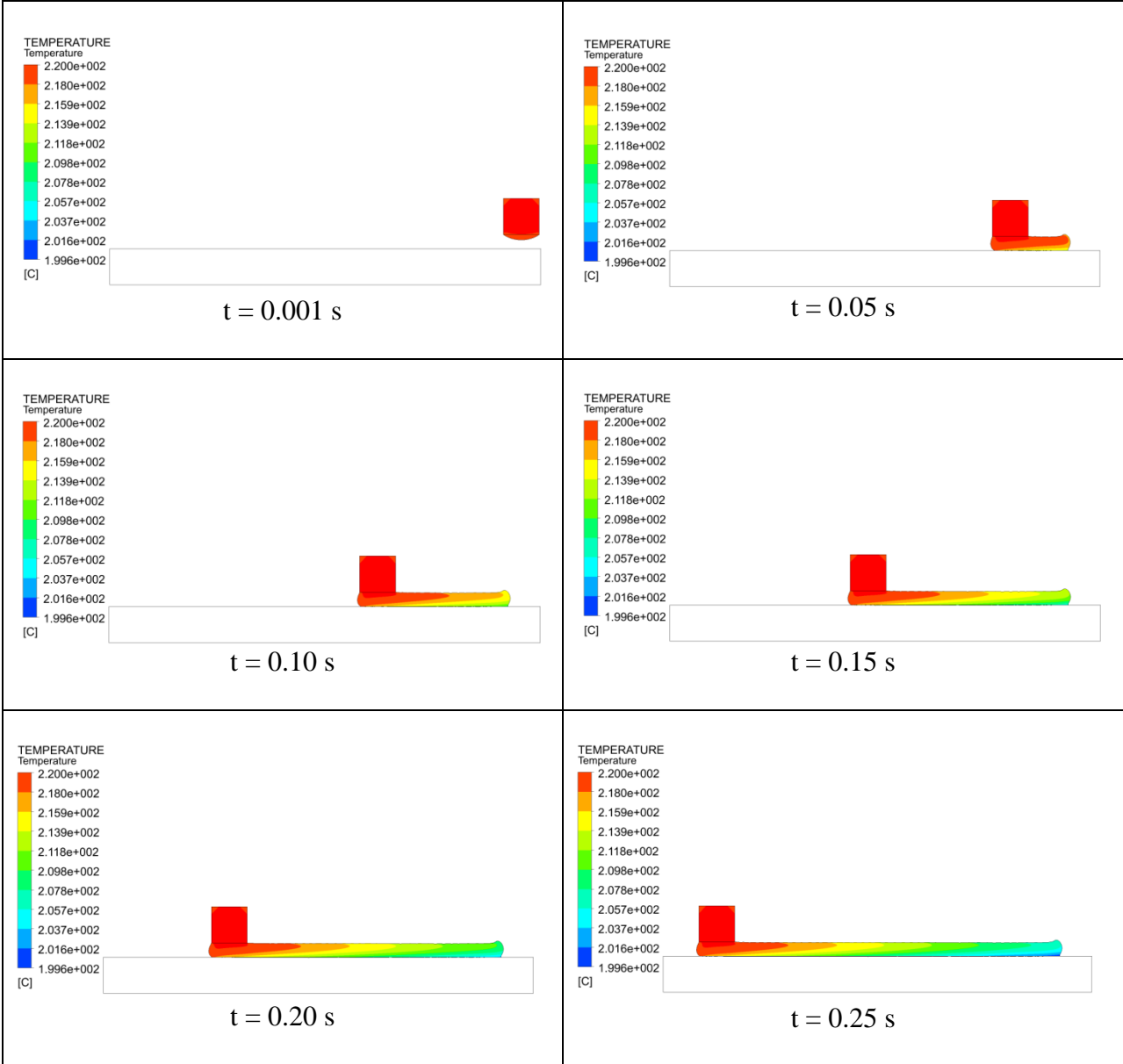
Fig. 8 Temperature distribution and deposited filament shape during the first layer deposition
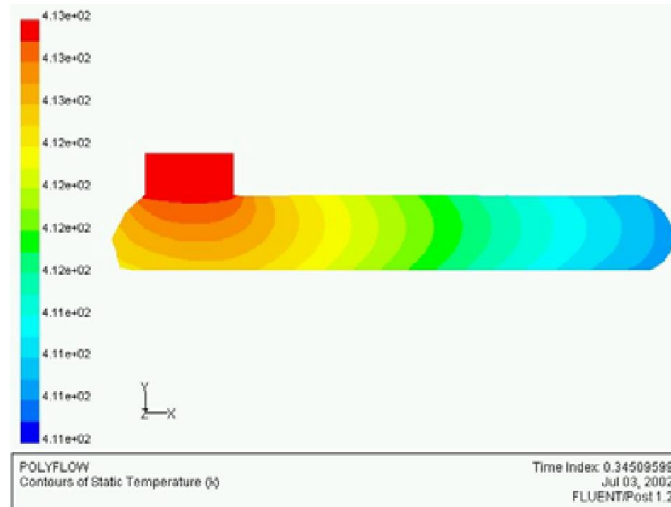
Fig. 9 Temperature distribution and deposited filament shape in Bellini's simulation model [6]

Table 3 Differences between the current and Bellini's simulation models

	Current Simulation Model	Bellini's Simulation Model [6]
Heat Transfer Coefficient of Build Platform	100 W/m^2-°C	10 W/m^2-°C
Deposition Speed	20 mm/s	5 mm/s
Deposition Time	0.25 s	0.35 s
Deposition Length	5 mm	1.75 mm
Temperature	T_{max} = 220.0 °C T_{min} = 199.6 °C ΔT = 20.4 °C	T_{max} = 140.0 °C T_{min} = 138.0 °C ΔT = 2.0 °C

The evolution of temperature distribution during the first layer cooling is shown in Figure 10. This step in the material extrusion process was simulated for 1.25 seconds to account for the horizontal movement of the printhead to its original location and the vertical movement of the build platform. In this simulation model, it was observed that the temperature of the first layer decreased from 220.0 °C to approximately 122.0 °C in 0.25 second, which was a 19.9% decrease.

The results were compared to the temperature profile of an ABS part measured using an infrared camera at Oak Ridge National Laboratory by Dinwiddie et al. [7]. In that study, a five-layer four-inch (101.6 mm) square was printed using a commercially available material extrusion additive manufacturing machine. The first layer was deposited at 170.0 °C and the temperature decreased to approximately 118.0 °C after 0.25 second, which was an 11.7% decrease. One of the reasons for the difference in percentage decrease could be due to the fact that the build platform in the simulation model was set to a slightly lower temperature than that at Oak Ridge National Laboratory. Since other critical information, such as the chamber temperature and deposition speed, were not provided in that study, it was difficult to determine other sources that caused the difference in percentage decrease. However, in both cases, exponential temperature

decays were observed, and it only took a fraction of a second for the temperature of the first layer to reach steady state during the cooling process.
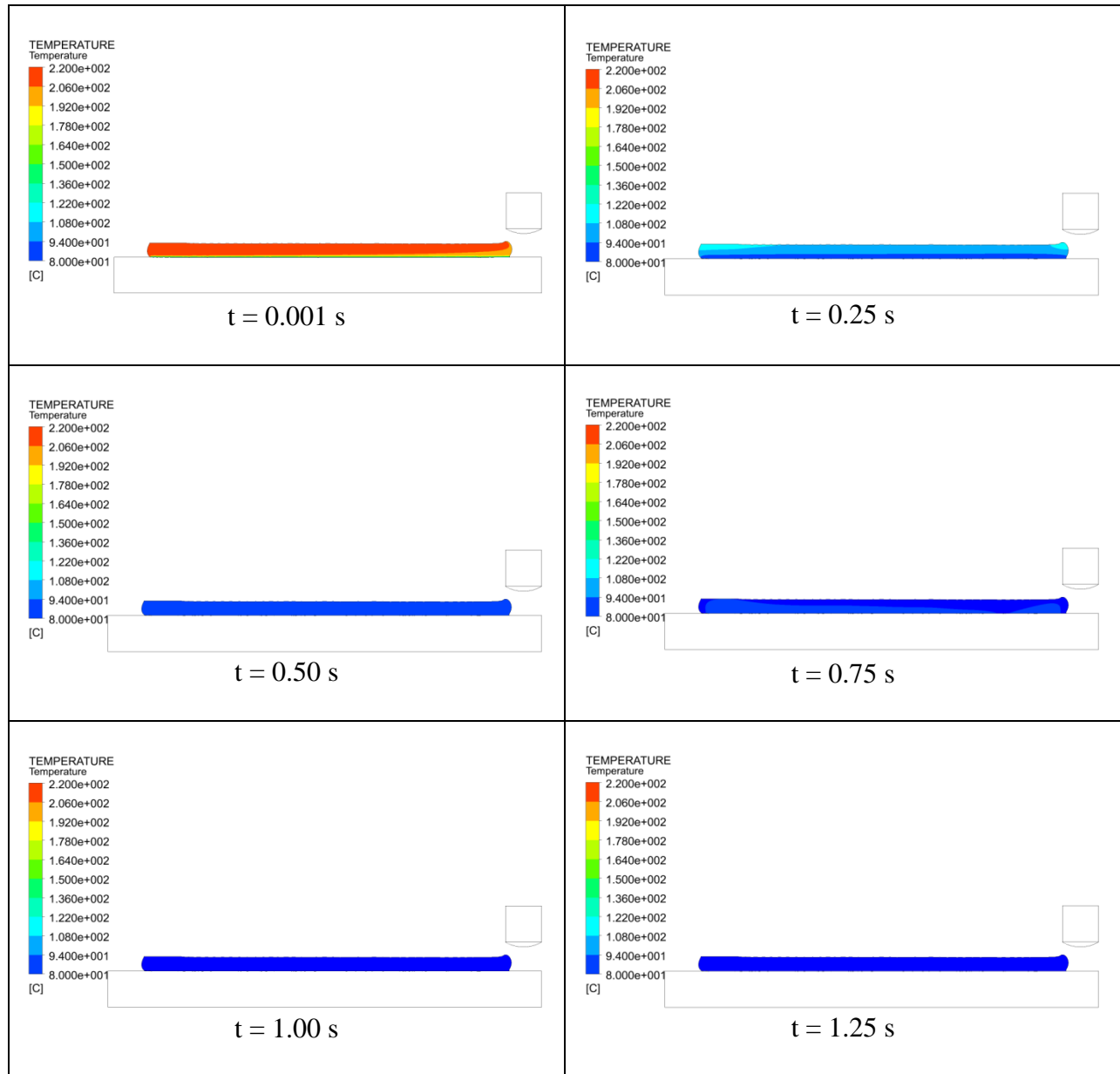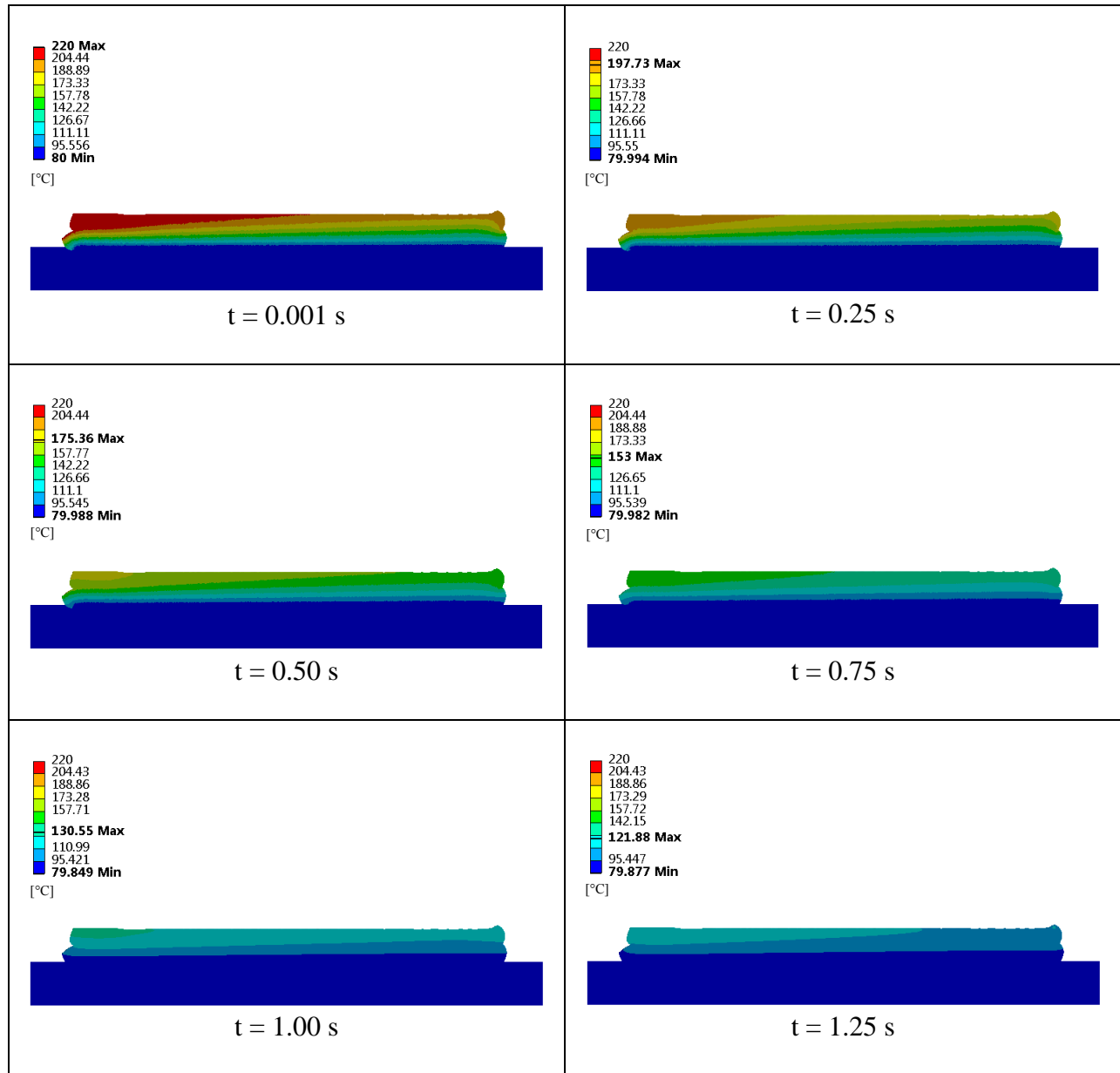

Fig. 10 Temperature distribution during the first layer cooling

The evolutions of temperature distributions and deposited filament shapes during the second layer deposition and the two-layer cooling are shown in Figures 11 and 12, respectively. As previously stated, the procedure for this simulation model was similar to that for the first layer deposition and cooling. However, the conduction heat transfer between the two layers was simulated using the fluid-to-fluid contact capability in ANSYS® Polyflow.
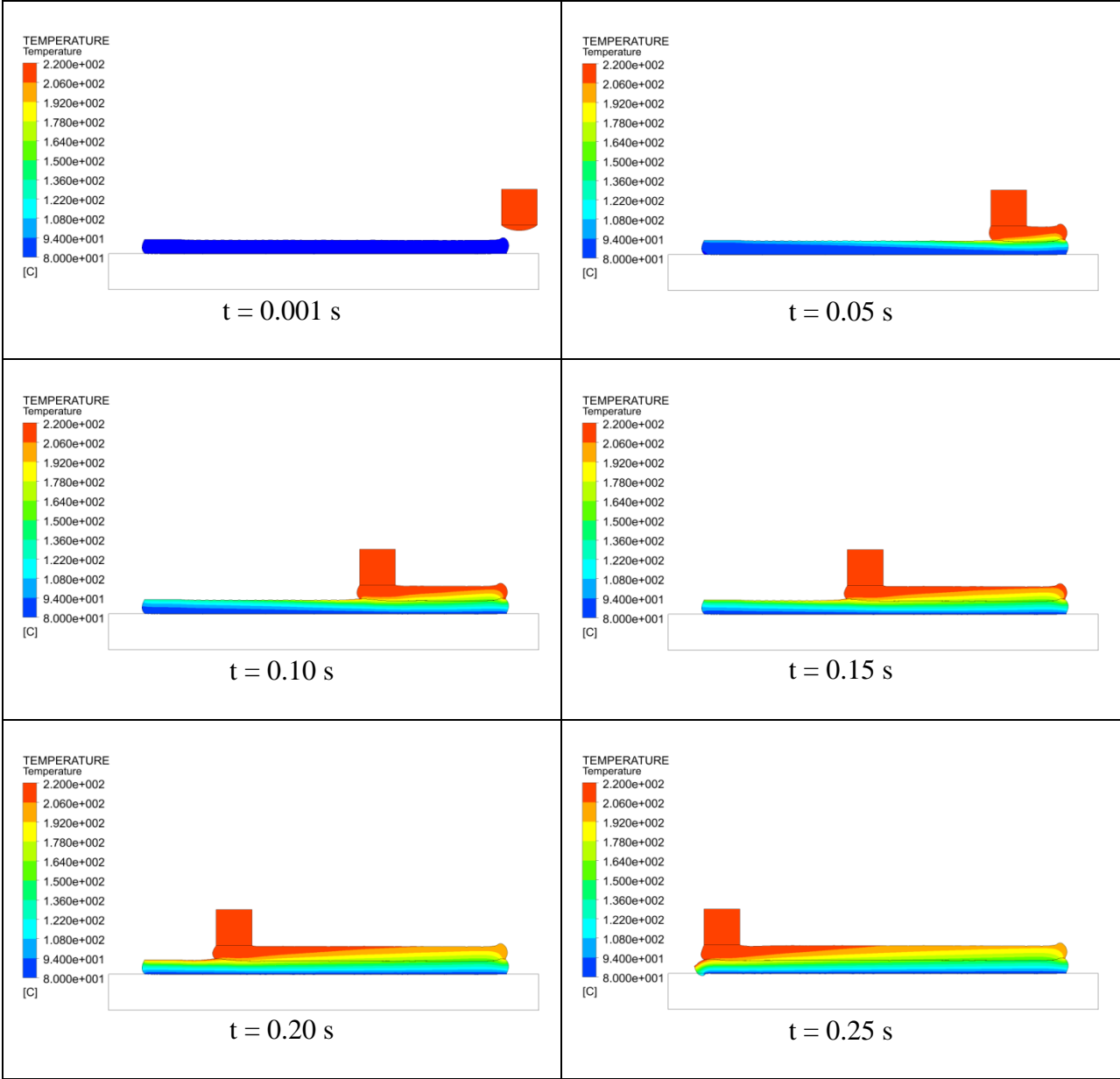
Fig. 11 Temperature distribution and deposited filament shape during the second layer deposition

Fig. 12 Temperature distribution during the two-layer cooling

The residual stress and warpage/deformation of the deposited two layers of filaments at steady state are presented in Figures 13 and 14, respectively. Since this simulation model was used to predict the thermally-induced residual stress and part warpage caused by the crystallization of the material during the cooling process, the two-layer cooling simulation model results were linked to conduct these structural analyses in ANSYS® Mechanical. These simulation model results were validated with experimental results as shown in Figure 14b, which is discussed in the following section.
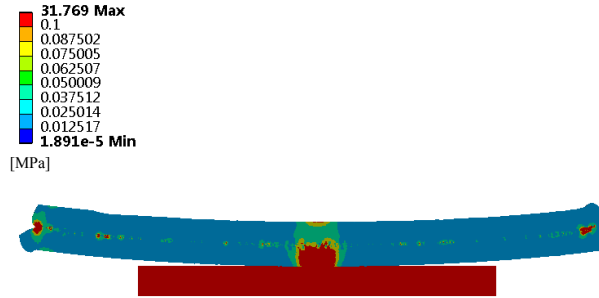
Fig. 13 Residual stress at steady-state

| (a) | (b) |
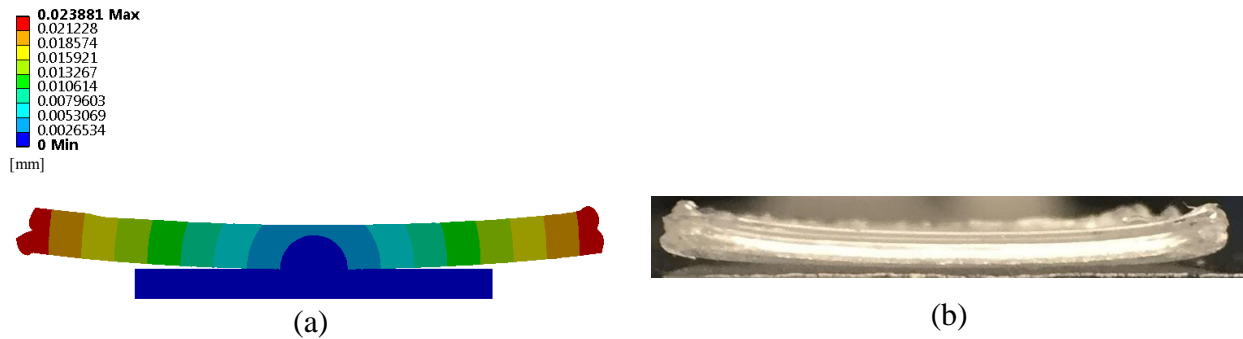
Fig. 14 Warpage/deformation at steady-state from (a) a simulation model and (b) an experiment

Validations and Parametric Studies of Warpage/Deformation Simulation Model

Two different geometries were used for the simulation models and experiments as shown in Figure 15. Since the simulation models were computationally intensive, two layers of filaments that were 5 mm in length were simulated, whereas five layers of filaments that were 20 mm in length were fabricated in the experiments. The fabrication of a larger part in experiments also facilitated the part warpage measurement using a caliper. However, these geometry differences led to differences in part warpage values between the simulation models and experiments as well. The experimental measurements, therefore, needed to be extrapolated in order to account for the geometry differences.

Simulation Models (2-D)	Experiments (3-D)

Fig. 15 Geometry differences in simulation models and experiments

First, in order to account for the differences in deposition length, the radius of curvature was considered. The radius of curvature, r, was calculated using Equation 5:

$$r = \frac{H}{2} + \frac{W^2}{8H} \tag{5}$$

where W is the deposition length and H is the measured warpage. Assuming the radius of curvature to be a constant, the warpage was then extrapolated by decreasing the deposition length to match with that of the simulation models. This extrapolation method is described using an example in Figure 16. In this example, the measured warpage from experiments was assumed to be 1 mm. The radius of curvature was calculated and plotted in blue. When the deposition length was decreased from 20 mm to 5 mm as in experiments to simulation models, the extrapolated warpage was calculated to be 0.06 mm, which was 94% less than the original value. The extrapolated warpage is plotted in red.
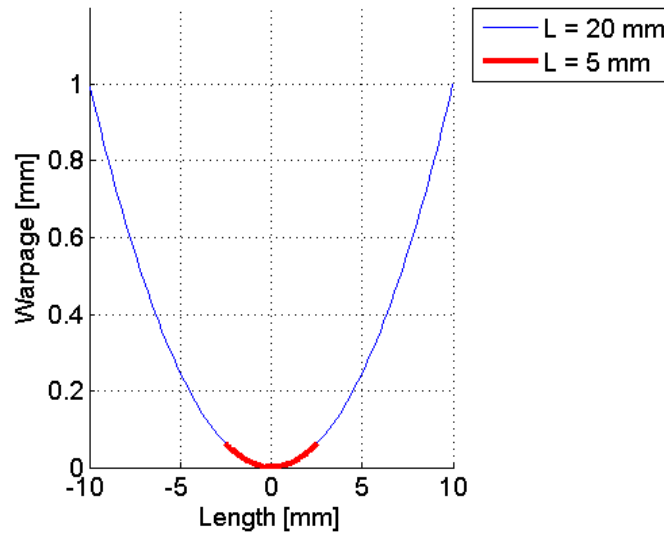
Fig. 16 Example plot of warpage vs. deposition length

In addition, the number of layers also affected the warpage since it was related to the number of repetition of heating and cooling the part experienced during the material extrusion process. Using the simulation models presented in the Results section of this paper, the warpage values were simulated by varying the number of layers from one to five. The results are plotted in Figure 17. As the number of layers decreased from five to two as in experiments to simulation models, the warpage decreased by 6% from 0.0253 mm to 0.0239 mm.
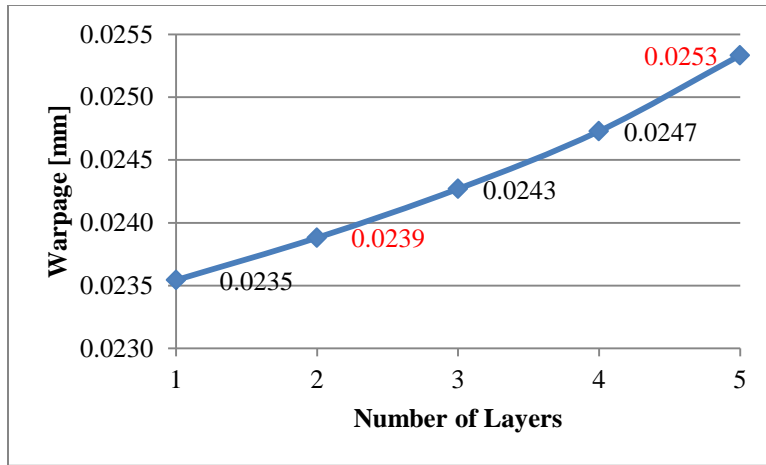
Fig. 17 Plot of warpage vs. number of layers from simulation models

The parametric studies of the warpage simulation model were conducted by applying the extrapolation methods to determine the effects of adjusting process variable settings on part warpage. The process variable settings, such as deposition temperature, deposition speed, and layer height, were varied using the values shown in Table 2.

The effect of increasing the deposition temperature from 200 °C to 240 °C was first determined. The plot of experimentally measured warpage at various deposition temperatures is shown in Figure 18, and the experimental and simulation model warpage values are summarized in Table 4. The extrapolated experimental results and simulation model results were comparable in values and followed the same trend. However, varying deposition temperature did not have significant effects on warpage.
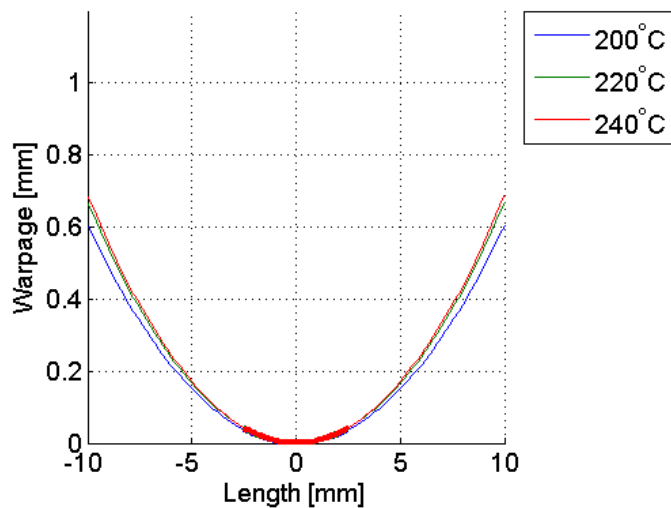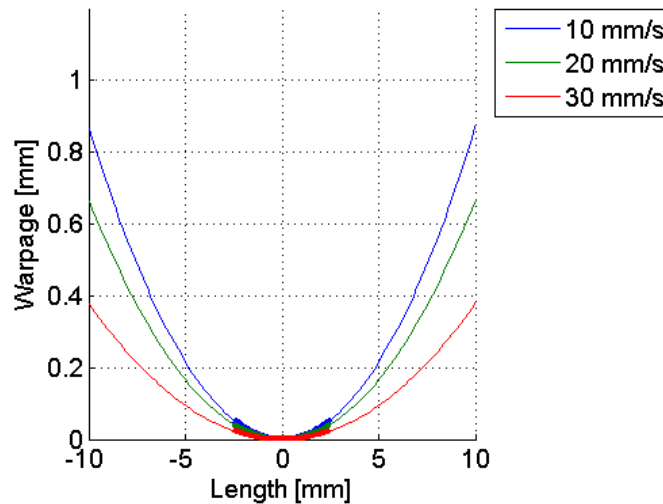

Fig. 18 Plot of experimental warpage with varying deposition temperature

Table 4 Experimental and simulation model warpage with varying deposition temperature

Process Variable Settings	Deposition Temperature		200 °C	220 °C	240 °C
	Deposition Speed		20 mm/s		
	Layer Height		0.2 mm		
Warpage	Experiment	Measured	0.61 ± 0.10 mm	0.67 ± 0.30 mm	0.69 ± 0.31 mm
		Extrapolated	0.0355 mm	0.0391 mm	0.0403 mm
	Process Simulation Model		0.0235 mm	0.0239 mm	0.0239 mm

The effect of increasing the deposition speed from 10 mm/s to 30 mm/s was also determined. The plot of experimentally measured warpage at various deposition speeds is shown in Figure 19, and the experimental and simulation model warpage values are summarized in Table 5. The extrapolated experimental results and simulation model results showed good correlations and followed the same trend, which was an increase in deposition speed led to a decrease in warpage. This phenomenon was likely related to the temperature gradient within each layer. With a lower deposition speed, a longer time was required for the deposition process to be completed for one layer. This led to a larger temperature gradient within that layer and therefore higher warpage. In contrast, with a higher deposition speed, it took a shorter time to complete the deposition of one layer. This led to a smaller temperature gradient within the layer and therefore lower warpage.
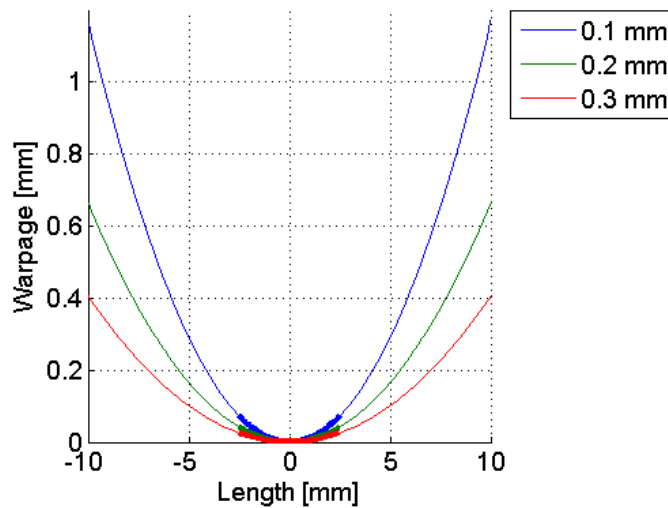

Fig. 19 Plot of experimental warpage with varying deposition speed

Table 5 Experimental and simulation model warpage with varying deposition speed

Process Variable Settings	Deposition Temperature		220 °C		
	Deposition Speed		10 mm/s	20 mm/s	30 mm/s
	Layer Height		0.2 mm		
Warpage	Experiment	Measured	0.87 ± 0.28 mm	0.67 ± 0.30 mm	0.38 ± 0.19 mm
		Extrapolated	0.0510 mm	0.0391 mm	0.0223 mm
	Process Simulation Model		0.0240 mm	0.0239 mm	0.0235 mm

Finally, the effect of increasing the layer height from 0.1 mm to 0.3 mm was determined. The plot of experimentally measured warpage at various layer heights is shown in Figure 20, and the experimental and simulation model warpage values are summarized in Table 6. The experimental results showed that an increase in layer height led to a decrease in warpage. This phenomenon was likely related to the temperature gradient within multiple layers. Since the number of layers was kept constant, a lower layer height resulted in a thinner fabricated part. This meant that a part with a lower layer height cooled more quickly compared to that with a higher layer height, which led to higher warpage. However, since a discrepancy existed between the experimental results and the simulation model results, further investigations are necessary.

Fig. 20 Plot of experimental warpage with varying layer height

Table 6 Experimental and simulation model warpage with varying layer height

Process Variable Settings	Deposition Temperature		220 °C		
	Deposition Speed		20 mm/s		
	Layer Height		0.1 mm	0.2 mm	0.3 mm
Warpage	Experiment	Measured	1.17 ± 0.59 mm	0.67 ± 0.30 mm	0.41 ± 0.20 mm
		Extrapolated	0.0682 mm	0.0391 mm	0.0240 mm
	Process Simulation Model		0.0248 mm	0.0239 mm	0.0242 mm

Conclusions

In this research, three types of material extrusion process simulation models were developed, which were the first layer deposition and cooling, the second layer deposition and cooling, and residual stress/warpage.

- The temperature distribution of the first layer was compared to material extrusion of ceramics conducted by Bellini. Temperature variations existed between the top and bottom surfaces, as well as in the deposition direction, between the two models. However, the results were comparable considering the differences in the heat transfer coefficient of build platform and the deposition speed. The cooling time of the first layer was also compared to the temperature profile of an ABS part measured using an infrared camera at Oak Ridge National Laboratory by Dinwiddie et al. In both cases, exponential temperature decays were observed, and the temperature distributions reached steady state in a fraction of a second. These simulation models that have the capabilities of predicting temperature distributions of deposited filaments will provide support in the developments of inter-layer bonding and mechanical property simulation models in the future.

- With regard to the warpage results, although the experimental measurements were extrapolated due to the differences in geometries, good correlations were shown between the extrapolated experimental results and simulation model results. In addition, when process variable settings were varied, the same trends in warpage were observed in most cases.

- In this research, the deposition and cooling simulation models were validated by comparison with literature results, and the warpage simulation model was validated by comparison with experimental data. The proposed material extrusion process simulation models provided promising results as the basis for screening new materials computationally.

References

1. Karl, M. *Plastics Portal*. 2016 [cited 2016 July 25]; Available from: http://www.isovolta.de/englisch/Kunststoffe.htm.
2. Turner, B.N., R. Strong, and S.A. Gold, *A Review of Melt Extrusion Additive Manufacturing Processes: I. Process Design and Modeling.* Rapid Prototyping Journal, 2014. **20**(3): p. 192-204.
3. Bellini, A., S. Guceri, and M. Bertoldi, *Liquefier Dynamics in Fused Deposition.* Journal of Manufacturing Science and Engineering, 2004. **126**(2): p. 237-246.
4. *HYREL System 30*. 2014 [cited 2014 December]; Available from: http://www.hyrel3d.com/.
5. Agarwala, M.K., et al., *Structural Quality of Parts Processed by Fused Deposition.* Rapid Prototyping Journal, 1996. **2**(4): p. 4-19.
6. Bellini, A., *Fused Deposition of Ceramics: A Comprehensive Experimental, Analytical and Computational Study of Material Behavior, Fabrication Process and Equipment Design*, 2002, Drexel University. p. 297.

7.   Dinwiddie, R.B., et al. *Infrared Imaging of the Polymer 3D-Printing Process*. in *SPIE*. 2014. Baltimore, Maryland.